DOI 10.1007/s11141-019-09926-5
Radiophysics and Quantum Electronics, Vol. 61, Nos. 8–9, January–February, 2019
(Russian Original Vol. 61, Nos. 8–9, August, 2018)

CHIMERA STRUCTURES IN THE ENSEMBLES OF NONLOCALLY COUPLED CHAOTIC OSCILLATORS

V. S. Anishchenko*and G. I. Strelkova

UDC 517.9+621.372

We study the structure and properties of the chimera states in the ensembles of chaotic oscillators with nonlocal coupling. It is shown that the phase and amplitude chimera states in the ensembles of chaotic oscillators with nonhyperbolic and hyperbolic attractors can be obtained using the models in the forms of two-dimensional Hénon and Lozi maps. The mechanisms of birth, the structure, and the lifetime of the phase and amplitude chimeras and the regime of solitary states are studied. The chimera states in two coupled ensembles of chaotic maps are considered. The possibility of realizing a new type of the chimera structure, namely, the chimera consisting of the solitary states is demonstrated. The effects of the external and mutual synchronizations of the chimera states are described by an example of two coupled ensembles of logistic maps with nonlocal coupling. A qualitative analogy of the obtained results with the classical effect of synchronization of periodic self-sustained oscillations is discussed.

1. INTRODUCTION

The studies of collective dynamics of the ensembles of various nature and the dissipative-structure formation in them have for several decades been in the focus of attention of the specialists in nonlinear dynamics of complex systems of interacting oscillators [1, 2]. It has been established that appearance of the synchronization clusters, spatial intermittency, and regular and chaotic spatiotemporal structures is typical of nonlinear ensembles. As a rule, many works studied the ensembles of identical oscillators with local or global coupling. New types of structures, called chimeras, have recently been discovered [3–5]. To a large extent, their appearance is due to introduction of the nonlocal coupling among the ensemble oscillators. Three types of coupling among the ensemble oscillators are considered in the chimera-state studies, namely, local, global, and nonlocal. In the case of local coupling, each ensemble element is symmetrically coupled with P right- and left-hand neighbor oscillators (in the one-dimensional ensemble, we have $P = 1$). In the case of global coupling, each oscillator is coupled with all ensemble oscillators on the right- and left-hand sides ($P = N/2$, where N is the number of ensemble oscillators). For the nonlocal coupling type, an individual oscillator is coupled with the finite number P of the neighbor right- and left-hand oscillators ($1 < P < N/2$). The chimera structures were observed for the first time in a one-dimensional ensemble of the nonlocally coupled phase oscillators [3] and then this effect was in more detail described in [4], in which the notion of the chimera states was proposed. The chimera structures are the clusters of a finite number of oscillators with incoherent (nonsynchronous) dynamics, which coexist with the clusters with coherent (synchronous) dynamics. The chimera spatiotemporal structures are characterized by distinct boundaries in the ensemble and are rather rough formations, i.e., do not disappear in the case of small perturbations of the ensemble parameters and the initial conditions.

* wadim@info.sgu.ru

N. G. Chernyshevsky Saratov National Research State University, Saratov, Russia. Translated from Izvestiya Vysshikh Uchebnykh Zavedenii, Radiofizika, Vol. 61, No. 8–9, pp. 739–753, August 2018. Original article submitted May 8, 2018; accepted September 21, 2018.

In recent years, the chimera structures have attracted attention of many researchers. Many works have been published in which numerical, theoretical [6–32], and experimental [33–38] results of chimera studies are reported. The chimera structures have been discovered in the ensembles containing various types of identical discrete and differential nonlinear oscillators [11, 12, 17, 29, 39]. Analysis of various spatiotemporal structures, including the chimera states in complex ensembles, is not only of fundamental value, but also of great practical significance. It is important when studying the Josephson-junction arrays [40], large arrays of the coupled lasers [41], the neural networks [42], the brain dynamics [43], power-supply networks [44, 45], and other systems.

In this work, we consider the chimera structures in the ensembles of nonlocally coupled chaotic oscillators with discrete time. Our studies have shown that choosing the ensembles of relatively simple one- and two-dimensional maps, we can study the phase and amplitude chimera structures, which are also realized in more complex ensembles of differential systems. However, in this case, the mathematical simulation of the ensemble dynamics becomes much simpler. This work presents a brief review of the results which have been obtained in recent years by the Division of Radio Physics and Nonlinear Dynamics at Saratov State University.

2. BASIC MODELS OF DISCRETE CHAOTIC SYSTEMS WITH HYPERBOLIC AND NONHYPERBOLIC ATTRACTORS

Detailed studies of the spatiotemporal structures in the ensembles of nonlocally coupled chaotic systems, both discrete and differential, show the conceptual dependence of the type of the realized structures on the type of chaotic attractors of the individual oscillators in the ensemble. It was established that certain spatiotemporal structures, including the chimera ones, are born in the ensembles consisting of chaotic oscillators with the nonhyperbolic type of chaotic attractors. In this case, the type and characteristics of the realized structures turn out to be similar for many studied systems. In the ensembles composed of the oscillators with hyperbolic (or, to be more exact, quasihyperbolic) attractors, other-type structures are realized and, which is the most important, the chimera structures are not usually born in such ensembles [27]. On the basis of numerous computer experiments, the two-dimensional Hénon and Lozi maps were introduced as the basic models [17, 46]. It is shown that they can be used to describe formation of the spatiotemporal structures including the chimera ones in a wide class of ensembles of nonlocally coupled oscillators. The Hénon and Lozi maps are described by discrete Eqs. (1) and (2), respectively:

$$x_{n+1} = 1 - \alpha x_n^2 + y_n, \qquad y_{n+1} = \beta x_n, \tag{1}$$

$$x_{n+1} = 1 - \alpha |x_n| + y_n, \qquad y_{n+1} = \beta x_n, \tag{2}$$

where n is the discrete time. Both maps are two-dimensional, and each map contains two control parameters α and β. The parameter α controls nonlinearity, while the parameter β characterizes the compression degree of the phase-space element on the plane of the phase variables (x, y).

Hénon system (1) realizes transition to chaos via the cascade of period-doubling bifurcations in accordance with the Feigenbaum universality. Born as a result of period doublings, the chaotic attractor is nonhyperbolic. It contains a theoretically infinite number of stable and unstable fixed points. This is due to the effects of homoclinic touching of the stable and unstable separatrices of the saddle points. According to the Afraimovich and Shil'nikov, such a type of chaotic attractor is called a quasi-attractor and characterized by multistability. The Hénon map qualitatively describes the dynamics of a fairly wide class of chaotic systems. Therefore, in the case of strong compression ($\beta \ll 1$), we obtain a one-dimensional logistic map. For spiral attractors in three-dimensional differential systems, the Poincaré map on the two-dimensional secant turns out to be topologically equivalent to the Hénon map [47]. As is evident from the studies, the ensembles of the Rössler and the Anishchenko–Astakhov oscillators realize the spatiotemporal structures from the logistic and cubic maps, such that these structures are similar to those observed in an ensemble of

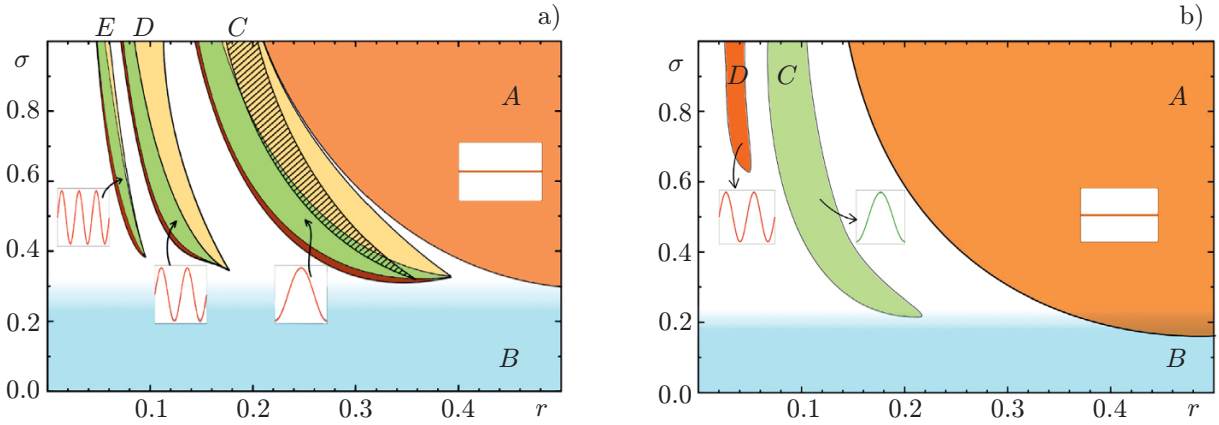

Fig. 1. Bifurcation diagrams for the ensembles of nonlocally coupled Hénon (*a*) and Lozi (*b*) maps. The figure inserts demonstrate instantaneous amplitude profiles, namely, a uniform profile (straight line) in the complete-synchronization region A and the amplitude profiles with one, two, and three maxima, which are realized with decreasing coupling radius r. Inside the regions C, D, and E, the period-doubling bifurcations take place with decreasing coupling force σ.

nonlocally coupled Hénon maps [12, 29].

Lozi map (2) demonstrates a hard transition to an almost hyperbolic chaotic attractor, which is the only one in the system phase space and does not include stable points. Multistability in the Lozi system is ruled out. For $\beta = 0$, the Lozi map is transformed to the one-dimensional tent map and simulates the dynamics of the differential three-dimensional systems with the Lorenz-type hyperbolic attractor in the Poincaré secant. Therefore, using the Hénon and Lozi maps as individual oscillators of the ensembles, one can describe the spatiotemporal structures in a sufficiently wide class of chaotic systems. Let us consider the dynamic and statistical characteristics of the spatiotemporal structures, which can be realized in the ensembles of nonlocally coupled Hénon and Lozi maps.

3. ENSEMBLE OF NONLOCALLY COUPLED HÉNON MAPS

Let us consider a one-dimensional ensemble that consists of N nonlocally coupled Hénon or Lozi maps with periodic boundary conditions, i.e., closed in a ring, and is described by the following equations:

$$x_i^{t+1} = f(x_i^t, y_i^t) + \frac{\sigma}{2P} \sum_{j=i-P}^{i+P} \left[f(x_j^t, y_j^t) - f(x_i^t, y_i^t) \right], \qquad y_i^{t+1} = \beta x_i^t. \tag{3}$$

Here, x^t and y^t are the real values of the phase variables, t is the discrete time, σ is the nonlocal-coupling coefficient, P is the number of the neighbor elements of the ensemble on the right- and left-hand sides of the element with the number i, $i = 1, 2, \ldots, N$ is the serial number of the element in the ensemble, and $N = 1000$. The functions $f(x_i, y_i)$ and $f(x_j, y_j)$ correspond to the right-hand side of the first equation of Hénon map (1) or map Lozi (2). The parameters of both maps have fixed values, namely, $\alpha = 1.4$ and $\beta = 0.3$. The initial conditions for the ensemble elements were chosen randomly distributed in a unit square.

Figure 1 shows the bifurcation diagrams for ensembles of the Hénon (Fig. 1*a*) and Lozi (Fig. 1*b*) maps on the plane of the parameters σ and $r = P/N$ (coupling radius). In Fig. 1*a*, the regions A, C, D, and E correspond to the regions of coherent dynamics of the Hénon-map ensemble and the region B characterizes the regime of spatiotemporal chaos. The gradient variation of color in the region B reflects gradual transition from the partial-synchronization regime (the white region in Fig. 1*a*) and the traveling-wave regime (the white region in Fig. 1*b*) to the spatiotemporal chaos. In the region A, the coherent regime corresponds to the regime of complete chaotic synchronization. If the coupling radius is fixed at the level $r = 0.16$, the chimera structures emerge in the ensemble for the coupling-coefficient values in the interval $0.20 \le \sigma \le 0.35$.

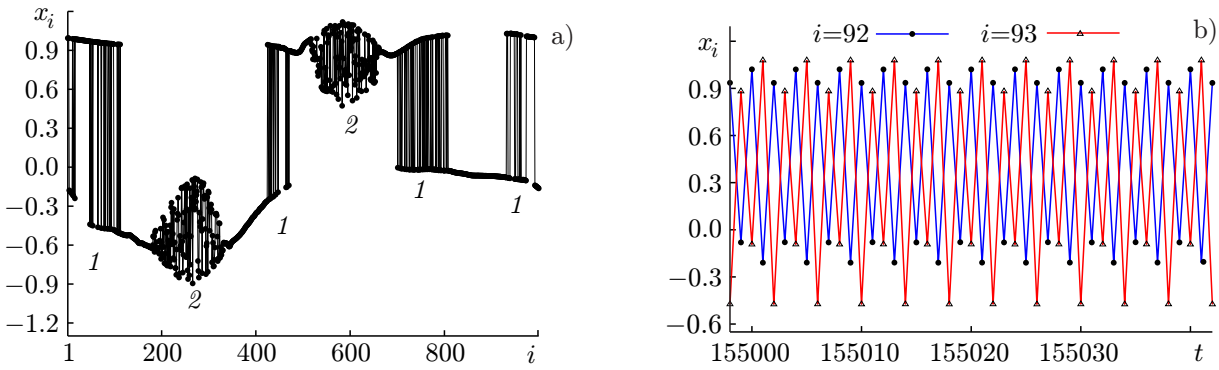

Fig. 2. The profile of the instantaneous amplitude values in the Hénon-map ring (3) with the phase and amplitude chimeras denoted as *1* and *2*, respectively (*a*) and shows the time realizations of the oscillations of two neighbor oscillators from the phase-chimera cluster, where the blue and red colors correspond to $i = 92$ and 93, respectively (*b*). The coupling parameters are $\sigma = 0.258$ and $r = 0.16$.

The studies have shown that two typical regimes, namely, the phase- and amplitude-chimera regimes are realized [29, 39].

Figure 2*a* shows the results of calculations of the instantaneous-amplitude profile for an ensemble of coupled Hénon maps, which illustrates the phase and amplitude chimeras.

The phase chimeras are the incoherent clusters (the regions *1* in Fig. 2*a*) and simultaneously coexist with two incoherent amplitude-chimera clusters (regions *2*) and several coherent clusters (the smooth-profile regions in Fig. 2*a*). The incoherence of the phase-chimera clusters manifests itself in that although the oscillators inside these clusters are characterized by periodic oscillations, they have the "phase" shift which is irregular along the cluster. Most frequently, this shift is equal to a half oscillation period (the time shift by one iteration). This is illustrated in Fig. 2*b*.

The phase shift among the oscillators inside the phase-chimera clusters is confirmed by the calculations of the normalized mutual-correlation coefficient, which irregularly varies for the phase-chimera cluster, taking the values $+1$ or -1 [20, 48]. Another pattern is observed for the amplitude chimera. The oscillators of the amplitude-chimera cluster are in the regime of the chaotic oscillations which are not correlated. Therefore, the amplitude chimera to the full extent corresponds to an uncorrelated (nonsynchronous) cluster in the ensemble. The oscillators of the amplitude-chimera cluster demonstrate the oscillation irregularity in time, which manifests itself in the effect of intermittency among several oscillation types [28]. This effect is represented by the time-irregular toggling among the chaotic oscillations, which reflect the amplitude-chimera dynamics, and the periodic oscillations, which are typical of the phase-chimera regime. Our studies have shown that the intermittency regime is observed for a sufficiently long but finite time, which determines the amplitude-chimera lifetime. Once this process is completed, all the oscillators belonging to the amplitude-chimera cluster switch to the long-living phase-chimera regime [28]. The fact that the amplitude chimera is characterized by the irregular toggling from one regime to the other (intermittency) and realized over a finite time interval refers this chimera type to the so-called transient chimeras [21].

The studies have shown that using the external noise action, one can control the amplitude-chimera lifetime and, in particular, make it significantly longer [28].

4. AN ENSEMBLE OF NONLOCALLY COUPLED LOZI MAPS

Let us consider the dynamics of ensemble (3), using the Lozi map as an individual oscillator in the ensemble. The studies [27, 46] show that in this ensemble, one can also observe transition from the regime of complete chaotic synchronization to that of the spatiotemporal chaos with varying nonlocal-coupling intensity. However, first, this transition is performed via the regime of the so-called solitary states and, second, the chimera-state regimes are not observed in this case. Let us consider the bifurcation diagram of the regimes for the Lozi ring, which is given in Fig. 1*b*.

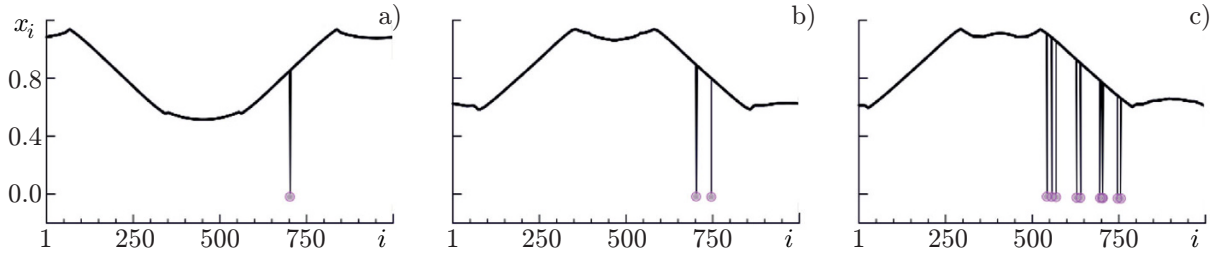

Fig. 3. The solitary-state regimes in the ring of coupled Lozi maps for $r = 0.2$ and decreasing coupling parameter σ: $\sigma = 0.226$ (a), 0.225 (b), and 0.223 (c). In the first case, one amplitude spike is observed (a) followed by two (b) and over (c) spikes.

This bifurcation diagram qualitatively resembles the diagram for the Hénon-map ring (see Fig. 1a) by the presence of the coherence regions A, C, and D and the spatiotemporal-chaos region B. However, the transition from the chaotic-synchronization region A to the region B is performed via the solitary-state regime, while the traveling-wave regimes are observed in the white-colored regions as in the ensemble of nonlocally coupled Lorenz oscillators [49]. Let us consider the solitary-state regime. If the transition from the region A to the region B is performed by varying the coupling parameter, the pattern shown in Fig. 3 is realized. For $\sigma = 0.226$, a sharp amplitude spike for one oscillator (see Fig. 3a) is observed in the instantaneous profile. A further decrease in the coupling parameter leads to an increase in the number of oscillators in the amplitude-spike regime (see Figs. 3b and 3c) and is completed by the transition to the spatiotemporal-chaos regime. It is noteworthy that the chimera structures are not realized during this transition. The mechanism of birth of the solitary-state regime is due to variation in the properties of the individual oscillators of the ensemble under the action of the signals from the neighbor oscillators because of the nonlocal coupling. According to our studies, the dynamics of the individual Lozi oscillator in the ensemble is considerably changed under the action of P neighbor left- and right-hand oscillators. Under the external action, the Lozi system ceases to be hyperbolic and becomes bistable. The amplitude jumps in Fig. 3 correspond to the phase-trajectory jump-over to the second attractor because of the random initial conditions. The attraction region of the second attractor increases with decreasing coupling coefficient σ. This results in an increase in the number of solitary states, which is shown in Fig. 3.

Let us consider this issue in more detail. Using simple transformations, Eq. (3) of the ring can be reduced to the form

$$x_i^{t+1} = (1-\sigma) f(x_i^t, y_i^t) + \frac{\sigma}{2P} \sum_{j=i-P}^{i+P} f(x_j^t, y_j^t), \qquad y_i^{t+1} = \beta x_i^t. \tag{4}$$

The obtained system (4) shows that the nonlocal-coupling influence leads to the fact that the coupling coefficient changes the individual-oscillator form, i.e., the multiplier $(1-\sigma)$ appears in front of the oscillator equation (the first term in Eq. (4)) and this oscillator operates in the nonautonomous regime under the action of the neighbor P oscillators (the second term) due to nonlocal coupling. As a result of these changes, the individual oscillators in the ensemble acquire essentially other properties. Special studies of the Lozi-map ring show that the individual oscillators in the ensemble take the following bistability properties due to action (4): another attractor emerges near the Lozi attractor, such that the attraction region of the new attractor is sufficiently small and enlarges with decreasing coupling coefficient. The calculation results are given in Fig. 4.

By virtue of the random nature of specifying the initial conditions, one ensemble oscillator falls within the narrow attraction basin (see Fig. 4a) and goes over to the solitary-state regime. As the coupling coefficient decreases, the attraction basins are enlarged (see Fig. 4b) and a still greater number of oscillators go over to the solitary-state regime. The number of such oscillators increases according to the linear law with decreasing coupling coefficient and becomes almost equal to N as the coupling coefficient tends to zero.

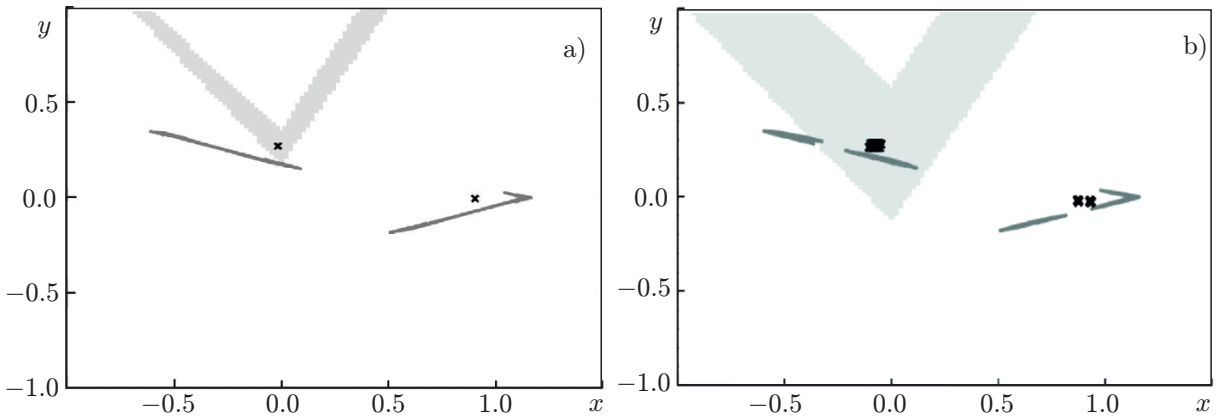

Fig. 4. Attractors of system (4) for various values of the coupling coefficient σ: $\sigma = 0.226$ (*a*) and 0.200 (*b*). The light-gray color is used to show the attraction basins of the attractors of the solitary states, which were calculated for the chosen oscillator of ensemble.

In the limiting case $\sigma = 0$, as it follows from Eq. (4), the system consists of the isolated Lozi oscillators such that each oscillator contains only the initial attractor. A new attractor, which corresponds to the solitary-state regime, disappears and the ensemble goes over the spatiotemporal-chaos regime.

5. CHIMERA OF THE SOLITARY STATES IN THE COUPLED ENSEMBLES OF HÉNON AND LOZI MAPS

Let us consider a system of two mutually coupled ensembles with nonlocal coupling that consists of the one-dimensional rings of Hénon and Lozi oscillators. The ensemble equations are written as follows:

$$x_i^{t+1} = f(x_i^t, y_i^t) + \frac{\sigma_1}{2P} \sum_{j=i-P}^{j+P} [f(x_j^t, y_j^t) - f(x_i^t, y_i^t)] + \gamma F_i^t, \qquad y_i^{t+1} = \beta x_i^t, \tag{5a}$$

$$u_i^{t+1} = g(u_i^t, v_i^t) + \frac{\sigma_2}{2R} \sum_{j=i-R}^{j+R} [g(u_j^t, v_j^t) - g(u_i^t, v_i^t)] - \gamma F_i^t, \qquad v_i^{t+1} = \beta u_i^t, \tag{5b}$$

where $i = 1, 2, \ldots, N$ and $N = 1000$. Systems of Eqs. (5*a*) and (5*b*) describe the ring of nonlocally coupled Hénon maps ($f(x, y) = 1 - \alpha x^2 + y$) and the ring of nonlocally coupled Lozi maps ($g(u, v) = 1 - \alpha |u| + v$) maps, respectively. Two rings are coupled via the coupling function F, which has the following form in the cases of dissipative and inertial couplings among the rings, respectively:

$$F_i^t = g(u_i^t, v_i^t) - f(x_i^t, y_i^t), \qquad F_i^t = u_i^t - x_i^t. \tag{6}$$

The coefficient γ characterizes the force of the symmetric coupling among the ith oscillators of Hénon and Lozi rings.

As a result of numerical studies, it has been established that all the spatiotemporal structures, which have been found by present time in the individual (uncoupled) Hénon and Lozi ensembles, can be realized in the considered system of Eqs. (5*a*) and (5*b*) during the parameter variation. Thus, for example, in the case of variation in the symmetric-coupling parameter γ, the regimes of the phase and amplitude chimeras can be realized in the Lozi ring, while the solitary-state and traveling-wave regimes in the ensemble space can be realized in Hénon ring. In addition to the above-mentioned structures, a new type of the chimera states, which are called the solitary-state chimeras and represents the chimera structure including the solitary states, can be realized in system of Eqs. (5*a*) and (*5b*) for both dissipative and inertial coupling types [50]. A new structure emerges in the ensemble of Hénon oscillators for a small coupling coefficient γ and its form is shown in Fig. 5.

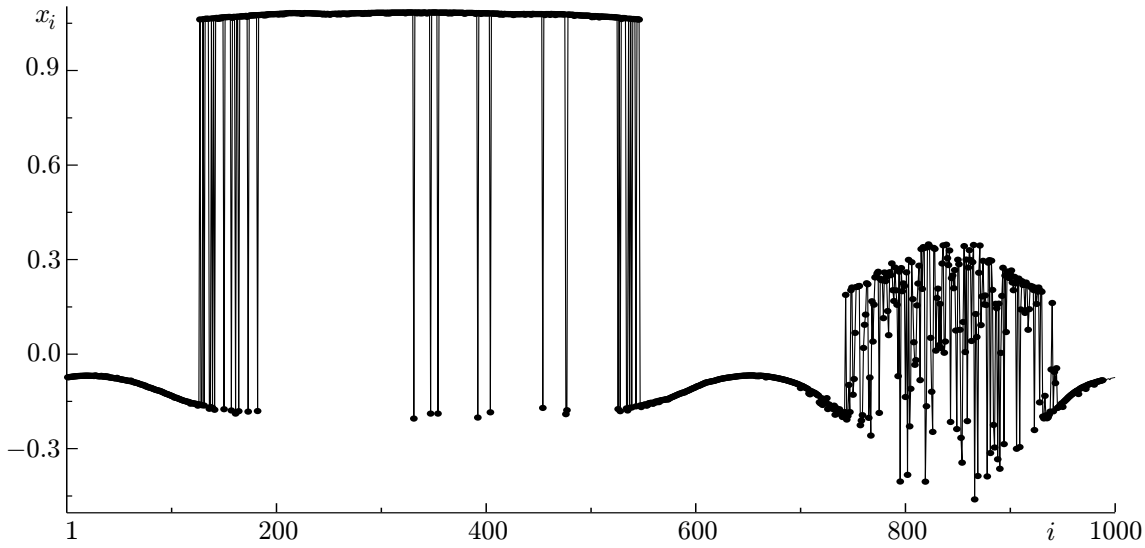

Fig. 5. Instantaneous profile of the dynamics of the Hénon-map ensemble in the coupled system of Eqs. (5*a*) and (5*b*), which illustrates the coexistence of the solitary-state chimera and the amplitude chimera for a small coupling coefficient $\gamma = 0.005$.

The incoherent cluster of the solitary-state chimera includes a group of oscillators ($300 < i < 500$ in Fig. 5) in the solitary-state regime, which operate in the chaotic regime as distinct from the phase chimera. The new structure is insensitive to the small variations in the initial conditions and realized in the finite region of variation in the control parameters of the system of Eqs. (5*a*) and (*5b*). The studies of the properties of the amplitude chimera in the system of Eqs. (5*a*) and (5*b*) of the coupled ensembles have shown complete compliance of its properties with the amplitude-chimera characteristics, which were described above for the solitary Hénon-map ring. The amplitude chimera is also characterized by the nonstationarity of oscillations in time for all oscillators the cluster and, as a rule, the lifetime finiteness. However, in a system of two coupled rings, the amplitude-chimera lifetime can be controlled in the wide range by varying the coupling coefficient γ. In this case, the lifetime dependence on the coupling parameter γ turns out to be essentially nonlinear.

6. EXTERNAL AND MUTUAL SYNCHRONIZATIONS OF THE CHIMERA STRUCTURES

The chimera-structure synchronization effects were studied by examples of the systems of coupled ensembles composed of various oscillators with the chaotic dynamics [50, 51]. For clarity, let us consider an example of the chimera-structure synchronization in a system of the two simplest coupled ensembles of the rings of logistic maps with nonlocal coupling using the parameter detuning. The equations of the system have the form

$$x_i^{t+1} = f_i^t + \frac{\sigma_1}{2P}\sum_{j=i-P}^{i+P}\left(f_j^t - f_i^t\right) + \gamma_{2\,1}F_i^t, \qquad y_i^{t+1} = g_i^t + \frac{\sigma_2}{2R}\sum_{j=i-R}^{i+R}\left(g_j^t - g_i^t\right) - \gamma_{1\,2}F_i^t,$$
$$f_i^t = \alpha_1 x_i^t\,(1 - x_i^t), \qquad g_i^t = \alpha_2 y_i^t(1 - y_i^t). \tag{7}$$

Here, α_1 and α_2 are the logistic-map nonlinearity parameters, σ_1 and σ_2 are the nonlocal-coupling coefficients, $P = R = 320$, $N = 1000$, $F_i^t = g_i^t - f_i^t$ is the function of the dissipative coupling of the rings, and $\gamma_{2\,1}$ and $\gamma_{1\,2}$ are the coefficients of coupling of the rings. For the external-synchronization regime, we have $\gamma_{2\,1} = 0$ and $\gamma_{1\,2} = \gamma$, whereas $\gamma_{2\,1} = \gamma_{1\,2} = \gamma$ for the mutual-synchronization regime.

Let us specify the parameters of the first and second rings such that various spatiotemporal structures can be realized in them in the absence of coupling. Let us fix the parameters, which are the same for the first and second rings ($R = P = 320$ and $N = 1000$), and choose the values $\alpha_1 = 3.7$, $\sigma_1 = 0.23$, $\alpha_2 = 3.85$, and

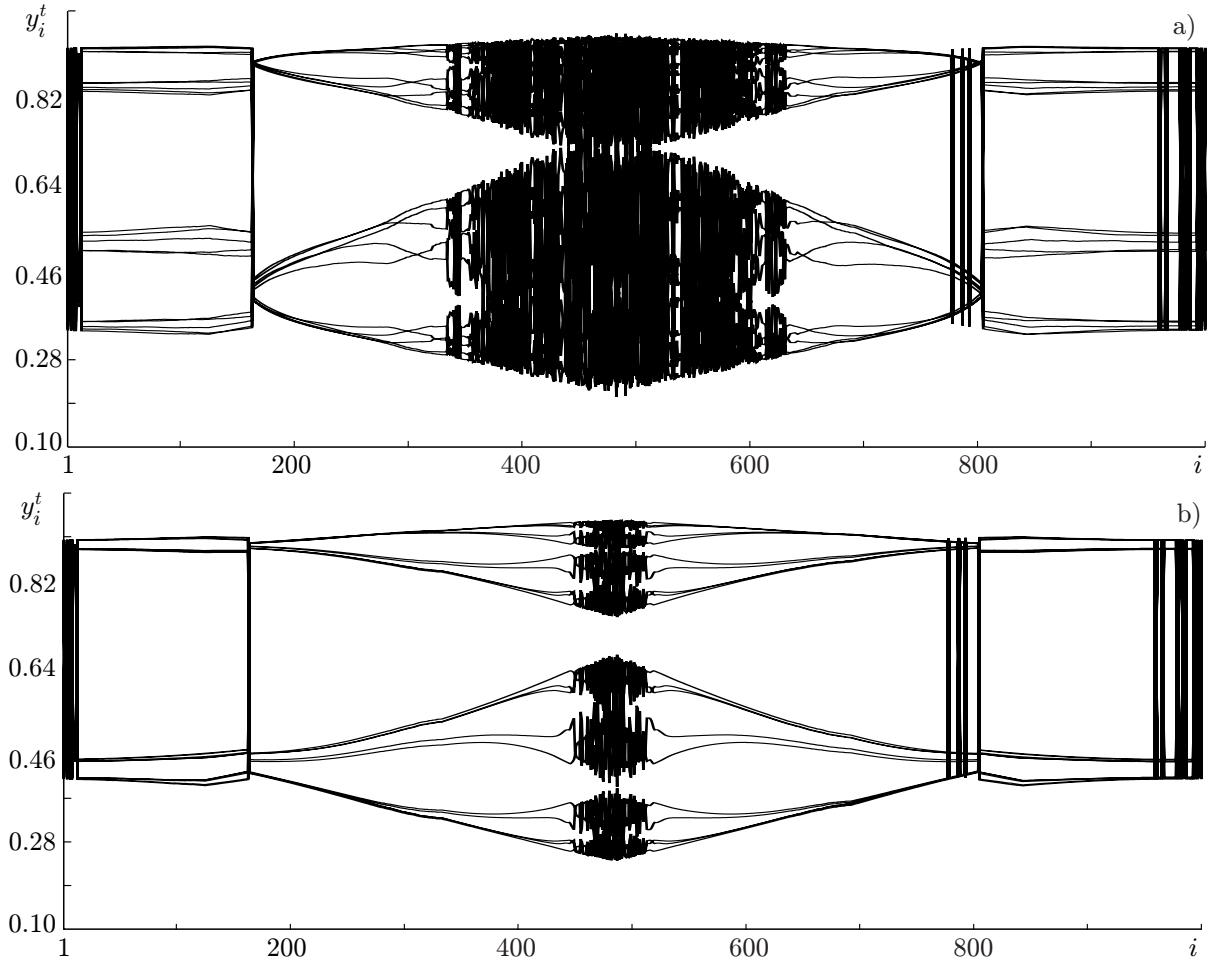

Fig. 6. Spatiotemporal profiles of the amplitude y_i^t in the second ring for the regimes of absence ($\gamma = 0.15$; *a*) and presence ($\gamma = 0.45b$) of the external-synchronization effect.

$\sigma_2 = 0.15$. In this case, the phase- and amplitude-chimera regimes are realized in the first ring in the absence of coupling of the rings, while the regime that is close to the spatiotemporal chaos is realized in the second ring for the above-mentioned parameters in the absence of coupling. The choice of the particular values of the above-mentioned parameters is not crucial. The main requirement for studying the synchronization effect is that the chosen parameter values should ensure the difference in the spatiotemporal structures of the rings in the absence of coupling.

Let us now follow the structure evolution in the second ring when introducing the unidirectional coupling. The calculations show that the spatial structures in the second ring change with introducing the coupling and increasing the quantity γ, and gradually approach the form of the initial structure of the control ring. Once the coupling coefficient reaches the value $\gamma = 0.40$ and over, the controlled-ring structure becomes identical to that in the control ring. This is illustrated in Fig. 6. Note that the dynamics of the elements of the coupled rings is shown in the figure using the spatiotemporal profiles, which represent the set of 100 latest instantaneous profiles of the ensemble states [29].

Strictly speaking, the results shown in Fig. 6 are insufficient to ascertain the effect of the chimera-structure synchronization. One should quantitatively substantiate the identity of the synchronous structures and demonstrate the existence of the finite synchronization region in the system-parameter space. The following mutual-correlation coefficient can be one of the possible quantitative characteristics of the

synchronous dynamics of two oscillators:

$$R_i = \frac{\langle \tilde{x}_i(t)\, \tilde{y}_i(t) \rangle}{\sqrt{\langle \tilde{x}_i^2(t) \rangle \, \langle \tilde{y}_i^2(t) \rangle}}, \tag{8}$$

where $\tilde{x}_i(t) = x_i(t) - \langle x_i(t) \rangle$, $\tilde{y}_i(t) = y_i(t) - \langle y_i(t) \rangle$, x_i and y_i are the oscillation amplitudes in the first and second coupled ensembles, respectively, the angle brackets denote time averaging, and $i = 1, 2, \ldots, N$ are the numbers of the corresponding elements of the interacting ensembles. The synchronous dynamics of the oscillators corresponds to the equality $R_i = 1.0$, whereas the coefficient R_i is smaller than unity in the absence of synchronization. The performed calculations indicate that the structure shown in Fig. 6*b* is actually identical to and, thus, synchronous with the initial structure, which is observed in the control ring in the absence of the inter-ring coupling. In this case, the mutual-correlation coefficient $R_i > 0.99$ and this condition is fulfilled in the finite region of the control-parameter variation. Therefore, it can be concluded that in the case of unidirectional coupling, the chimera structure of the first (control) ring synchronizes the structure in the second (controlled) ring and the effect of external synchronization of the chimera structures is realized.

The experiment whose results are given in Fig. 7 is more instructive. Let us fix $\alpha_2 = 3.85$ in the controlled ring and construct the synchronization region on the plane of two parameters, namely, the coupling coefficient γ and the nonlinearity parameter α_1 of the control ring. The variations in the parameter α_1 change the form of the spatiotemporal structures in the control ring. According to the calculations, the control-ring structures, which are realized in the case of variation in the parameter α_1, synchronize the similar structures in the controlled ring with increasing coupling coefficient γ. Then, varying the coupling coefficient, we calculate the mutual-correlation coefficient R_i and construct the synchronization region, which is shown in Fig. 7. In the hatched region A, we have $R_i > 0.99$. Therefore, the structures, which are totally synchronous with the structures in the control ring, are realized in the A region. In this case, it should be noted that during variations in the parameters α_1 and γ, different structures are observed inside the A region in Fig. 7 because of the parameter α_1 variation in the control ring. However, the structures in the first and the second rings are identical and synchronous everywhere in the A region.

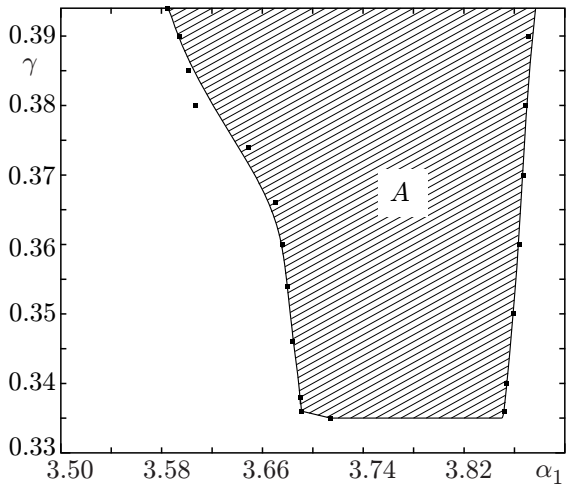

Fig. 7. The region of external synchronization of the spatiotemporal structures in system (7) on the parameter plane (α_1, γ) for $\alpha_2 = 3.85$, $\sigma_1 = 0.23$, and $\sigma_2 = 0.15$. In the hatched region A, the coefficient of mutual correlation of oscillations of the oscillators x_i^t and y_i^t is equal to $R_i > 0.99$.

To study the mutual synchronization of the chimera structures, we introduce the symmetric bidirectional coupling to Eq. (7) of the coupled ring by putting $\gamma_{1\,2} = \gamma_{2\,1} = \gamma$. Introducing a slight detuning for the parameters α_1 and α_2 in the ensembles of logistic maps, in the absence of coupling we obtain different chimera structures in the first and the second rings (see Fig. 8*a*). As it follows from the calculations, once the coupling is introduced, the structures start to converge and become synchronized for $\gamma > 0.07$ (see Figs. 8*b* and 8*c*).

The calculations of the mutual-correlation coefficient show that this condition is also fulfilled in the synchronization regime $R_i > 0.99$ in the finite region of the coupling-coefficient variation. Therefore, one can speak of realization of the effect of mutual synchronization of the chimera structures in the coupled ensembles described by Eq. (7). Note that the synchronous structures do not coincide with the structure forms in the first and the second ensembles in the absence of coupling, which is well seen in Fig. 8.

The above-described synchronization effect can qualitatively be compared with classical synchronization effect of periodic self-sustained oscillations. Indeed, in the case of external and mutual synchronization of the limit cycle, the spectral line of oscillations at the frequency ω can be considered as the simplest structure. Then, in the case of external synchronizations, the behavior of the external (master) oscillator is characterized by the spectral line at the frequency ω_1, while the structure of the slave-controlled oscillator, by the spectral line at the frequency ω_0. In the synchronization region, the frequency-locking effect is realized and these frequencies coincide.

In the case of mutual synchronization of the oscillators with close frequencies ω_1 and ω_0, a similar phenomenon is observed with the only difference that the frequency ω_1 or ω_0 or a certain intermediate frequency in the range $\omega_1 < \omega < \omega_0$ can be set in the synchronization region. According to the results presented in Sec. 5, a qualitatively similar pattern is realized in the case of interaction of two ensembles of nonlinear oscillators. For external synchronization, the spatiotemporal structure of the control ensemble ensures locking of the controlled-ensemble structure, and the synchronous-structure identity is preserved in the synchronization region. In the case of mutual synchronization, the mutual locking of the structures in the coupled ensembles is performed. In this case, the synchronized structures differ from the initial structures in the ensembles in the absence of coupling (see Fig. 8), which is also observed during the mutual synchronization of the coupled periodic oscillators.

The results shown in Fig. 7 also support the possibility of comparing the effect of synchronization of the spatiotemporal structures with the classical effect of the limit-cycle synchronization. The external-synchronization region in Fig. 7 qualitatively resembles the region of external synchronization of the limit cycle on the external-action amplitude–frequency detuning plane. In the case of the mutually coupled ensembles, the role of the action amplitude is played by the coupling coefficient γ, while that of the frequency detuning, by the parameter α_1 for the fixed parameter α_2. As distinct from the limit-cycle synchronization, in the case of the ensemble synchronization, we deal with the synchronization threshold with respect to the coupling parameter γ (see Fig. 7). The threshold presence is explained by the nonidentity of the interacting ensembles and the threshold level is a function of the nonlocal-coupling radius (the numbers R and P in Eq. (7)).

The above-performed comparison allows one to consider the results of synchronization of the chimera states as generalization of the concepts of the classical theory of synchronization of the periodic self-sustained oscillations to the case of synchronization of the spatiotemporal structures in the systems of the coupled ensembles of nonlinear oscillators.

7. CONCLUSIONS

In this work, it has been established that the Hénon and Lozi maps can be the basic models for describing the dynamic properties of the one-dimensional ensembles of chaotic systems with nonlocal coupling. The results of the analysis of the dynamics of the ensembles composed of Hénon and Lozi maps have been presented. It has been shown that the phase and amplitude chimera states [29, 39] are realized in the Hénon ensembles in the regime of nonhyperbolic chaos. The structure, properties, and correlation characteristics of the phase and amplitude chimeras have been described briefly. In [28], it is shown that the amplitude chimera in a solitary ensemble is characterized by the finite lifetime, which can be controlled using the noise action. In the Lozi-map ensembles, the traveling-wave and solitary-state regimes are realized, but the chimera-state regimes do not emerge [27, 46]. The mechanism of appearance of the solitary-state regime due to bistable dynamics of the ensemble elements because of the nonlocal-coupling influence has been discussed.

The above-given results totally correspond to the data available in the literature. Thus, all the spatiotemporal structures similar to those emerging in the Hénon ensemble are realized in the one-dimensional ensembles of nonlocally coupled R$\acute{}$ossler oscillators, Anishchenko–Astakhov oscillators, and logistic and cubic maps [12, 29]. The results of studying the dynamics of a one-dimensional ensemble of nonlocally coupled Lorenz oscillators in the regime of almost hyperbolic chaos [17] also totally correspond to the results which were discussed in this work for the ensemble of the Lozi oscillators. Therefore, the basic models of the

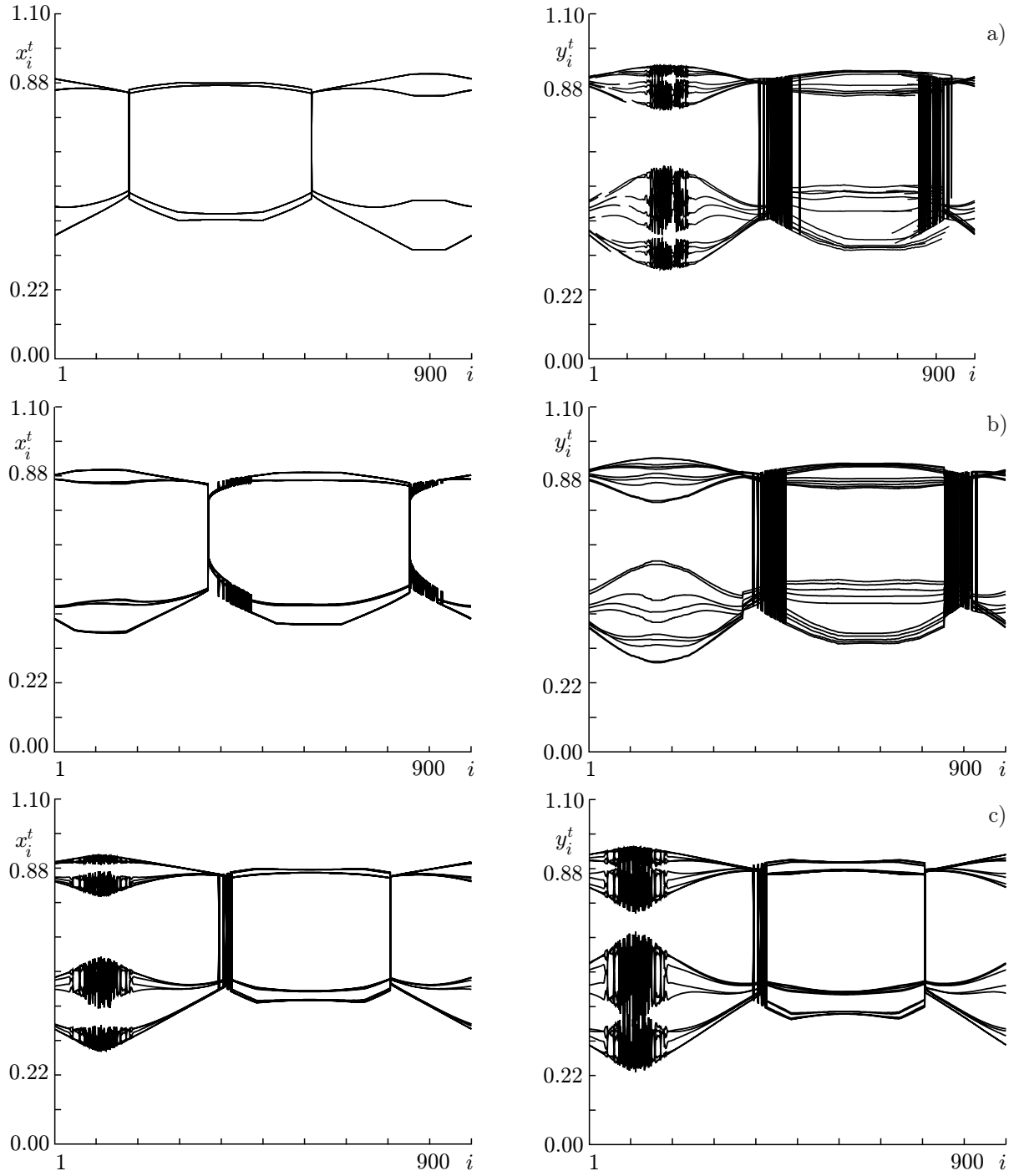

Fig. 8. Effect of mutual synchronization of the chimera structures in the symmetrically coupled ensembles x_i^t (the left-hand column) and y_i^t (the right-hand column) for various values of the coupling parameter γ equal to $\gamma = 0.000$ (*a*), 0.025 (*b*), and 0.075 (*c*) for $\alpha_1 = 3.70$, $\alpha_2 = 3.85$, and $\sigma_1 = \sigma_2 = 0.28$.

chaotic Hénon and Lozi oscillators do allow one to analyze a wide class of ensembles of nonlocally coupled chaotic oscillators.

We have also considered the case of two mutually coupled one-dimensional ensembles composed of the nonlocally coupled chaotic maps of various types. In this case, a new chimera-structure type (solitary-state chimera), which includes a finite number of oscillators in the solitary-state regime as an incoherent cluster, has been described.

In Sec. 6, we have considered the effects of external and mutual synchronizations of the chimera structures by an example of two coupled ensembles of logistic maps. The obtained results have been compared with and shown to be analogous to the conclusions of the classical theory of synchronization of the periodic self-sustained oscillations.

This work was supported by the German Physical Society (project No. SFB 910) and the Ministry of Education and Science of the Russian Federation within the framework of the state assignment (project No. 3.8616.2017/8.9).

REFERENCES

1. V. S. Afraimovich, V. I. Nekorkin, G. V. Osipov, and V. D. Shalfeev, *Stability, Structures and Chaos in Nonlinear Synchronization Networks*, World Scientific, Singapore (1995).
2. G. V. Osipov, J. Kurths, and Ch. Zhou, *Synchronization in Oscillatory Networks*, Springer, Berlin (2007).
3. Y. Kuramoto and D. Battogtokh, *Nonlinear Phenom. Complex Syst.*, **5**, No. 4, 380 (2002).
4. D. M. Abrams and S. H. Strogatz, *Phys. Rev. Lett.*, **93**, No. 17, 174102 (2004).
5. M. J. Panaggio and D. M. Abrams, *Nonlinearity*, **28**, R67 (2015).
6. D. M. Abrams, R. E. Mirollo, S. H. Strogatz, and D. A. Wiley, *Phys. Rev. Lett.*, **101**, 084103 (2008).
7. C. R. Laing, *Phys. Rev. E*, **81**, 066221 (2010).
8. E. A. Martens, C. R. Laing, and S. H. Strogatz, *Phys. Rev. Lett.*, **104**, 044101 (2010).
9. A. E. Motter, *Nat. Phys.*, **6**, 164 (2010).
10. M. Wolfrum and O. E. Omel'chenko, *Phys. Rev. E*, **84**, 015201 (2011).
11. I. Omelchenko, Y. Maistrenko, P. Hövel, and E. Schöll, *Phys. Rev. Lett.*, **106**, 234102 (2011).
12. I. Omelchenko, B. Riemenschneider, P. Hövel, Y. Maistrenko, and E. Schöll, *Phys. Rev. E*, **85**, 026212 (2012).
13. Y. Maistrenko, A. Vasylenko, O. Sudakov, et al., *Int. J. Bifurc. Chaos*, **24**, 1440014 (2014).
14. A. Zakharova, M. Kapeller, and E. Schöll, *Phys. Rev. Lett.*, **112**, 154101 (2014).
15. A. Yeldesbay, A. Pikovsky, and M. Rosenblum, *Phys. Rev. Lett.*, **112**, 144103 (2014).
16. D. Dudkowski, Y. Maistrenko, and T. Kapitaniak, *Phys. Rev. E*, **90**, 032920 (2014).
17. N. Semenova, A. Zakharova, E. Schöll, and V. Anishchenko, *Europhys. Lett.*, **112**, 40002 (2015).
18. S. Olmi, E. A. Martens, S. Thutupalli, and A. Torcini, *Phys. Rev. E*, **92**, 030901(R) (2015).
19. J. Hizanidis, E. Panagakou, I. Omelchenko, et. al., *Phys. Rev. E*, **92**, 012915 (2015).
20. T. E. Vadivasova, G. I. Strelkova, S. A. Bogomolov, and V. S. Anishchenko, *Chaos*, **26**, 093108 (2016).
21. F. P. Kemeth, S. W. Haugland, L. Schmidt, et al., *Chaos*, **26**, 094815 (2016).
22. S. Ulonska, I. Omelchenko, A. Zakharova, and E. Schöll, *Chaos*, **26**, 094825 (2016).
23. N. I. Semenova, A. Zakharova, V. Anishchenko, and E. Schöll, *Phys. Rev. Lett.*, **117**, 01410 (2016).
24. E. Schöll, *Eur. Phys. J. Spec. Top.*, **225**, 891 (2016).
25. V. Semenov, A. Zakharova, Y. Maistrenko, and E. Schöll, *Europhys. Lett.*, **115**, 10005 (2016).
26. J. Sawicki, I. Omelchenko, A. Zakharova, and E. Schöll, *Eur. Phys. J. Spec. Top.*, **226**, 1883 (2017).
27. E. Rybalova, N. Semenova, G. Strelkova, and V. Anishchenko, *Eur. Phys. J. Spec. Top.*, **226**, 1857 (2017).

28. N. I. Semenova, G. I. Strelkova, V. S. Anishchenko, and A. Zakharova, *Chaos*, **27**, 061102 (2017).
29. S. A. Bogomolov, A. V. Slepnev, G. I. Strelkova, et al., *Commun. Nonlinear Sci. Numer. Simul.*, **43**, 25 (2017).
30. M. S. Santos, J. D. Szezezh Jr., A. M. Batista, et al., *Phys. Lett. A*, **379**, 2188 (2015).
31. A. Zakharova, N. Semenova, V. Anishchenko, and E. Schöll, *Chaos*, **27**, 114320 (2017).
32. I. A. Shepelev, A. V. Bukh, T. E. Vadivasova, et al., *Commun. Nonlinear Sci. Numer. Simul.*, **54**, 50 (2018).
33. A. M. Hagerstrom, T. E. Murphy, R. Roy, et al., *Nat. Phys.*, **8**, 658 (2012).
34. M. R. Tinsley, S. Nkomo, and K. Showalter, *Nat. Phys.*, **8**, 662 (2012).
35. L. Larger, B. Penkovsky, and Y. L. Maistrenko, *Phys. Rev. Lett.*, **111**, 054103 (2013).
36. E. A. Martens, S. Thutupalli, A. Fourriere, and O. Hallatschek, *Proc. Natl. Acad. Sci. USA*, **110**, 10563 (2013).
37. T. Kapitaniak, P. Kuzma, J. Wojewoda, et al., *Sci. Rep.*, **4**, 6379 (2014).
38. L. Larger, B. Penkovsky, and Y. Maistrenko, *Nat. Commun.*, **6**, 7752 (2015).
39. S. A. Bogomolov, G. I. Strelkovva, E. Schöll, and V. S. Anishchenko, *Tech. Phys. Lett.*, **42**, No. 7, 765 (2016).
40. S. Watanabe, S. H. Strogatz, H. S. J. van der Zant, and T. P. Orlando, *Phys. Rev. Lett.*, **74**, 379 (1995).
41. R. D. Li and T. Erneux, *Phys. Rev. A*, **49**, 1301 (1993).
42. J. Hizanidis, N.E. Kouvaris, G. Zamora-López, et al., *Sci. Rep.*, **6**, 19845 (2016).
43. N. C. Rattenborg, C. J. Amlaner, and S. L. Lima, *Neurosci. Biobehav. Rev.*, **24**, 817 (2000).
44. A. E. Motter, S. A. Myers, M. Anghel, and T. Nishikawa, *Nat. Phys.*, **9**, 191 (2013).
45. T. Nishikawa and A. E. Motter, *New J. Phys.*, **17**, 015012 (2015).
46. N. I. Semenova, E. V. Rybalova, G. I. Strelkova, and V. S. Anishchenko, *Reg. Chaot. Dyn.*, **22**, 148 (2017).
47. V. S. Anishchenko, *Complex Oscillations in Simple Systems* [in Russian], Nauka, Moscow (1990).
48. T. E. Vadivasova, G. I. Strelkova, S. A. Bogomolov, and V. S. Anishchenko, *Tekh. Phys. Lett.*, **43**, No. 1, 118 (2017).
49. V. Dziubak, Y. Maistrenko, and E. Schöll, *Phys. Rev. E*, **87**, 032907 (2013).
50. A. Bukh, N. Semenova, E. Rybalova, et al., *Chaos*, **27**, 111102 (2017).
51. A. V. Bukh, G. I. Strelkova, and V. S. Anishchenko, *arXiv*, 1802.02771v1 (2018).